Title

The capricious nature of iodine catenation in I
2
excess, perovskite-derived hybrid Pt(
iv
) compounds

Journal

Chemical Communications, 55(5)

ISSN

1359-7345 1364-548X

Authors

Evans, Hayden A
Andrews, Jessica L
Fabini, Douglas H
et al.

Publication Date

2019

DOI

10.1039/c8cc07536k

Peer reviewed

Journal Name

ARTICLE TYPE

Cite this: DOI: 10.1039/xxxxxxxxxx

The capricious nature of iodine catenation in I_2 excess, perovskite-derived hybrid Pt(IV) compounds

Hayden A. Evans,[ab] Jessica L. Andrews,[a] Douglas H. Fabini,[bc‡] Molleigh B. Preefer,[ab] Guang Wu,[a] Anthony K. Cheetham,[bd] Fred Wudl,[c] and Ram Seshadri[abc]

Received Date
Accepted Date

DOI: 10.1039/xxxxxxxxxx

www.rsc.org/journalname

Perovskite-derived hybrid platinum iodides with the general formula $A_2Pt^{IV}I_6$ (*A* = formamidinium FA and guanidinium GUA) accommodate excess I_2 to yield hydrogen-bond-stabilized compounds where the I_2 forms catenates with I^- anions on the PtI_6 octahedra.

The bonding of atoms of the same element into a series — the phenomenon of catenation — is commonly associated with certain second and third period main group elements such as boron, carbon, sulfur, and phosphorous. This tendency is governed by multiple factors including mean bond-dissociation energy, sterics, electronegativity, and orbital hybridization.[1] Generally, catenation occurs less frequently as one moves down the periodic table as orbitals grow more diffuse and bonding strength decreases. An exception would be catenated iodides (commonly referred to as polyiodides, although the term oligoiodide is perhaps more appropriate), which are numerous and demonstrate great diversity in length as well as in structure. At this time, the Cambridge Crystallographic Data Center (CCDC) lists approximately 1600 structures containing some form of an I–I–I linkage with three or more I atoms. Examples of solid-state oligoiodide materials include molecular salts where triodide (I_3^-) subunits are charge balanced by counter cations, and connected frameworks where many oligoiodide moieties (I_2, I_3^-, I_5^-, I_7^-, I_9^-, *etc*) link together.[2,3]

[a]*Department of Chemistry and Biochemistry, University of California Santa Barbara, California 93106 United States. E-mail: seshadri@mrl.ucsb.edu*
[b]*Materials Research Laboratory, University of California Santa Barbara, California 93106 United States*
[c]*Materials Department, University of California Santa Barbara, California 93106 United States*
[d]*Department of Materials Science and Engineering, National University of Singapore, Singapore 117575, Singapore*
‡*Present address: Department of Nanochemistry, Max Planck Institute for Solid State Research, Heisenbergstr. 1, 70569 Stuttgart, Germany*
† Electronic Supplementary Information (ESI) available. This includes experimental details, crystallographic files (CCDC 1864903–1864907), structure descriptions, PXRD, TGA, DSC, and band structure information]. See DOI: 10.1039/b000000x/

Recently, some of us reported the crystallographic structure of a rare iodine homopolymer in a pyrroloperylene-iodide compound, reminiscent of the elusive starch-iodine complex.[4] The variety of oligoiodide structures results from favorable donor-acceptor interactions, and the many cations, anions, and solvent molecules that appear to impact these interactions in the solid state.

Donor-acceptor properties of iodine find many applications, including for increasing the conductivity of organic metals and conducting polymers,[5] enhancing the efficiency of dye-sensitized solar cells,[6,7] and improving the photocatalysis of materials for hydrogen evolution.[8,9] Recent interest in iodide-based perovskite photovoltaic materials[10–12] has engendered reports of incorporating I_3^- subunits into a hybrid bismuth iodide compound in order to introduce intergap electronic states that red-shifted the band gap.[13] This result is interesting in light of most Bi–I solar energy materials displaying relatively large bandgaps regardless of structure.[14] Materials that contained neutral I_2 molecules linking discrete $[BiI_6]^{3-}$ octahedra have also been noted to display direct bandgaps of ≈1.3 eV.[15] However, it was stated that covalency between the I_2 and $[BiI_6]^{3-}$ iodides did not appear to be present, and the structure should not be viewed as a $[BiI_6]^{3-}$–I_2–$[BiI_6]^{3-}$ 1D chain. This suggests that simple iodine/iodide proximity, not covalency, was enough to induce favorable properties of these materials in the solid state.

Here we present the findings that the hydrogen-bonded framework perovskite-derived materials, $(FA)_2PtI_6$ and $(GUA)_2PtI_6$ (FA = formamindinium and GUA = guanidinium), which were recently studied as members of an A_2PtI_6 series,[16] can be recrystallized as excess I_2 containing compounds. The new compounds, $(FA)_2PtI_6{\bullet}2I_2$ and $(GUA)_8(PtI_6)_3[PtI_4(I_3)_2]{\bullet}2I_2$, are described herein. In order to understand how size and hydrogen bonding tendencies impact the formation of these oligoiodide materials, a dimethylammonium (DMA) Pt-I compound was also prepared and studied. The solid $(DMA)_3PtI_6(I_3)$ provides valuable insight into how hydrogen bonding is essential to stabilizing this class of halide structures. Interestingly, all three materials,

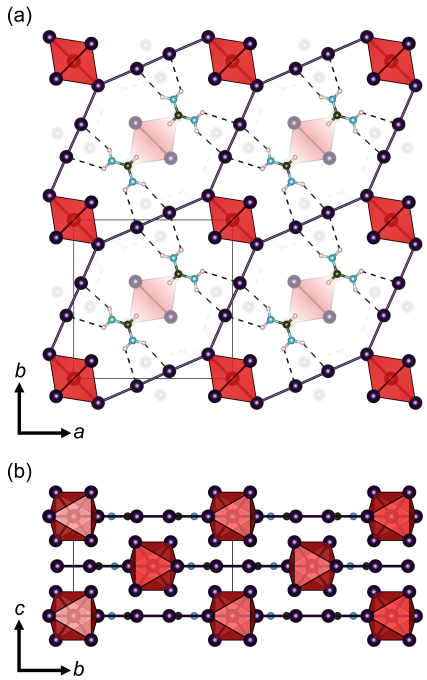

Fig. 1 Crystal structure of $(FA)_2PtI_6{\bullet}2I_2$ at 100 K. Atom color key; Pt = Red, I = purple, N = blue, C = black, H = white. (a) Depiction of the 1D chains forming between the iodides on the $[PtI_6]^{2-}$ octahedra and I_2 molecules. Hydrogen bonding columns that form between the FA cations and the I_2 molecules are displayed with dashed lines. The pertinent bond lengths are: I_2 molecule 2.77 Å; I_2–I^- 3.30 Å; N-H$\cdots$$I_2$ 3.0 Å. (b) Side view of the 2D sheets that are found parallel to the *ab* plane.

despite their distinct dimensionalities, display similar optical absorption profiles.

The structures of the hybrid platinum poly/oligoiodide materials, $(FA)_2PtI_6{\bullet}2I_2$, $(GUA)_8(PtI_6)_3[PtI_4(I_3)_2]{\bullet}2I_2$, and $(DMA)_3PtI_6(I_3)$, are presented in Figures 1 and 2. Figure 1 (a) emphasizes the intriguing 1D polyiodide chains that form in $(FA)_2PtI_6{\bullet}2I_2$ between apical iodides of the $[PtI_6]^{2-}$ octahedra and the I_2 molecules, as well as the 1D hydrogen bonding columns that form between the FA cations and the same I_2 molecules. Figure 1 (b) depicts the sheet-like structure formed by the I_2–$[PtI_6]^{2-}$ chains and the columns of FA cations and I_2 molecules. Compounds which present I_2 molecules or polyiodide moieties in donor-acceptor interactions with metal halide octahedra, similar to the aforementioned I_2–$[BiI_6]^{3-}$ system, are fairly common,[2,17–19] but the infinite 1D I_2–I–I_2 chain that extends through the structure of $(FA)_2PtI_6{\bullet}2I_2$ is to our knowledge the first example reported with such short distances between atoms.[20] By convention, covalent bonds between iodine/iodide atoms should have an interatom distance of no greater than 3.30 Å.[2] At 300 K, the single crystal X-ray diffraction measured distance of the I_2–I^- *bond* in $(FA)_2PtI_6{\bullet}2I_2$ is 3.32 Å, and at 100 K it is 3.30 Å. If we adhere to the 3.30 Å cutoff, only the low temperature structure of $(FA)_2PtI_6{\bullet}2I_2$ qualifies as a polyiodide material, but as we later demonstrate via Raman spectroscopy, this material displays vibrations indicative of a polyiodide material at 300 K. Furthermore, at both 300 K and 100 K, the I_2 intermolecular bond lengths are longer than the known solid-state I_2 bond distance of 2.67 Å (2.75 Å and 2.77 Å, respectively) suggesting that between 300 K and 100 K the donor apical iodides of the $[PtI_6]^{2-}$ octahedra are decreasing the I_2 I–I bond order. This is in agreement with a molecular orbital (MO) description of this compound,[21] which shows that the highest occupied molecular orbital (HOMO) has some degree of antibonding character.

Additionally, we note the significance of certain characteristics of the FA cations in $(FA)_2PtI_6{\bullet}2I_2$. Firstly, they are ordered, which is unlike the "tumbling" FA and methylammonium cations in $APbI_3$ perovskites.[22–25] Secondly, they hydrogen bond explicitly with the I_2 molecules and not the $[PtI_6]^{2-}$ iodides, as seen in the parent compound, $(FA)_2PtI_6$. If one considers both the FA cation arrangement, and the I_2 molecules location relative to the apical iodides on the $[PtI_6]^{2-}$ octahedra, one can see that these are potential structural signatures of halogen bonding.[26] In halogen bonding, covalently bonded, easily polarizable halogen atoms (like iodine) can form nucleophilic (negative) and electrophilic (positive) sides, with the electrophilic side being denoted as the "σ-hole." We have calculated the electron localization function (ELF) and electrostatic potential for $(FA)_2PtI_6{\bullet}2I_2$, and discuss the results in the last section of this work, as well as in the ESI.†

Figure 2 (a) shows the structure of $(GUA)_8(PtI_6)_3[PtI_4(I_3)_2]{\bullet}2I_2$ with organic cations omitted for clarity emphasizing the observed secondary I$\cdots$I bonding network (see ESI† for Figures with organic cation locations). Secondary I$\cdots$I bonds are interactions that are often seen in oligoiodide networks, and occur at distances between the previously mentioned cutoff for I–I covalent bonds, 3.30 Å, and the I$\cdots$I van der Waals distance, 3.9 Å.[2] In $(GUA)_8(PtI_6)_3[PtI_4(I_3)_2]{\bullet}2I_2$ there are three crystallographically independent Pt sites, each with distinct local enviornments. These three Pt octahedral enviornments are denoted in Figure 2 (a) and (b) with differing colors as well as bolded numbers (**1**–**3**) which coincide with the .cif file Pt label assignments. **1** refers to the $[PtI_6]^{2-}$ octahedra that have no close I$\cdots$I secondary bonding associations, **2** to the $[PtI_6]^{2-}$ octahedra that have two close secondary I$\cdots$I bonding associations with I_3 ligands of the $[PtI_4(I_3)_2]^{2-}$ moieties, and **3**, which refers to the $[PtI_4(I_3)_2]^{2-}$ moieties. The species **3**, in addition to forming secondary I$\cdots$I bonding associations with **2**, also forms secondary bonds with I_2 molecules in the *ab*-plane.† Figure 2 (b) illustrates one such secondary-bonding chain that forms between **3** and **2**, with bond lengths of the I_3 subunit (3.12 Å and 2.80 Å) from species **3** denoted. The occurance of **3** is quite interesting, because to our knowledge, no similar Pt or other metal based moiety has been reported to date. The labeled bond lengths are reminiscent of other asymmetric I_3^- anion bonds [2.7(1) Å and 3.2(1)],[27] and, as we demonstrate below, the Raman spectrum displays signatures of the I_3 subunit. As to the GUA cations, they form a complex and extensive hydrogen bonding network almost exclusively with $[PtI_6]^{2-}$ octahedra iodides.† Each of the four crystallographically independent GUA cations connect **1**, **2**, and **3** together, each in a distinct way, but with uncanny similarity to the GUA cations in its parent compound, $(GUA)_2PtI_6$.† This suggests that in addition to the secondary iodide network, the hydrogen bonding network is a considerable structural stabilizer.

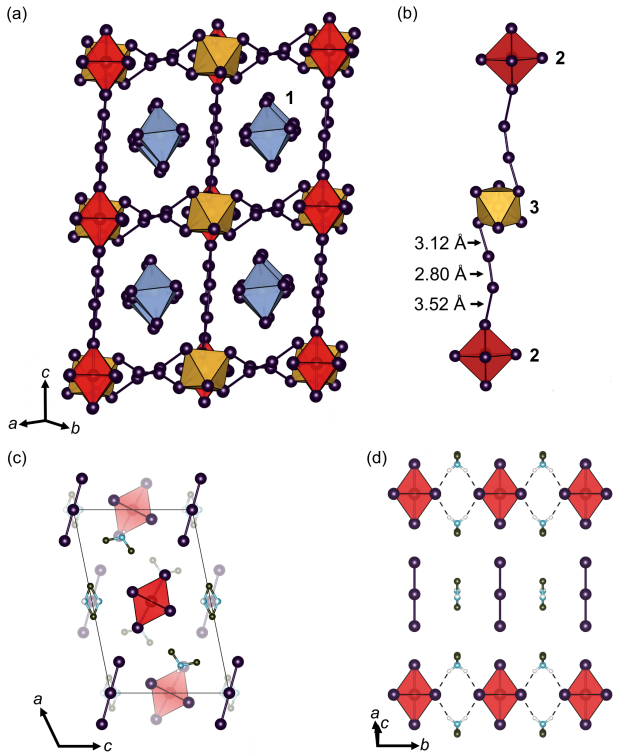

Fig. 2 The crystal structures of [(a) and (b)] $(GUA)_8(PtI_6)_3[PtI_4(I_3)_2]\bullet 2I_2$ and [(c) and (d)] $(DMA)_3PtI_6(I_3)$ at 100 K. Atom color key; I = purple, N = blue, C = black, H = white. (a) View of the $(GUA)_8(PtI_6)_3[PtI_4(I_3)_2]\bullet 2I_2$ structure with organic cations omitted for clarity, so as to better display the oligoiodide network. To signify crystallographic independence, the Pt octahedra colors are varied and labeled with bolded numbers **1**-**3** in the $(GUA)_8(PtI_6)_3[PtI_4(I_3)_2]\bullet 2I_2$ structure. (b) View of the crystallographically observed $[PtI_4(I_3)_2]^{2-}$ moiety **3** that forms secondary bonding chains along the *c*-axis with $[PtI6]^{2-}$ octahedra **2**. (c) View of $(DMA)_3PtI_6(I_3)$ down the *b*-axis. Hydrogen atoms are included on the DMA cations that are ordered, as these cations hydrogen bond with nearby $[PtI_6]^{2-}$ octahedra. (d) View of $(DMA)_3PtI_6(I_3)$ depicting the hydrogen bonding interactions between DMA cations and $[PtI_6]^{2-}$ octahedra, as well as the arrangement of I_3^- anions relative to the nearby $[PtI_6]^{2-}$ octahedra. The distance between apical $[PtI_6]^{2-}$ iodides and nearby I_3^- is 3.49 Å.

Figures 2 (c) and (d) illustrate the structure of $(DMA)_3PtI_6(I_3)$, where Figure 2 (c) shows the arrangement of $[PtI_6]^{2-}$ octahedra, I_3^- moieties, as well as the two distinct types of DMA cations; one that is ordered and one that is not. Figure 2 (d) shows the hydrogen bonding of the ordered DMA, where the N–H···I hydrogen bond lengths are at a distance of 2.87 Å and N to I distances are 3.68 Å; these are considered to be medium/strong interactions based on previous neutron diffraction studies.[28] The I_3^- moieties are aligned with the $[PtI_6]^{2-}$ octahedra at a distance of 3.49 Å (secondary I···I bonding).[2] Initially, we sought to make a DMA-containing A_2PtI_6 compound to juxtapose the materials $(FA)_2PtI_6$ and $(GUA)_2PtI_6$. We believed this $(DMA)_2PtI_6$ compound, with a cation roughly the size of FA but with less than half the hydrogen bonding sites, would better inform us as to the impact of hydrogen bonding in these halide materials. It was our intention to recrystallize this hypothetical $(DMA)_2PtI_6$ compound and observe the differences in I_2 inclusion. However, the $(DMA)_2PtI_6$ compound could not be isolated, and only the compound, $(DMA)_3PtI_6(I_3)$, formed. Though not our original intention, this raises a significant question: "Why did $(DMA)_2PtI_6$ not form?" In our previous report,[16] we discussed how the substantial hydrogen bonding capacity of the FA and GUA moieties engaged as structural guides. We believe that the similar size but reduced hydrogen bonding capacity of the DMA cation (compared to the FA cation) serves as a prime example to the significance of hydrogen bonding in these lower dimensional halide materials. Namely, that without a cation that can form numerous attractive H···I interactions, the electrostatic forces between cation and anion are not sufficient to stabilize a A_2PtI_6 molecular salt.

Raman spectra illustrate the I–I bonding character of these compounds, and are presented in Figure 3 (a). Two $[PtI_6]^{2-}$ octahedron Pt–I vibrations of varying strengths can be seen at 141 cm^{-1} and 156 cm^{-1} in all samples tested.[29] The other vibrations of interest are near 125 cm^{-1} and 180 cm^{-1}, which are attributed to the vibrations of I_3^- and I_2, respectively.[2] When classifying the polyiodide character of $(FA)_2PtI_6\bullet 2I_2$, the absence of a strong I_2 vibration near 180 cm^{-1} is quite telling, as this vibration will shift to lower energies if the I_2 molecule is acting as an acceptor. The amount of shift will depend on the strength of the respective donor species.[30] It is likely that for $(FA)_2PtI_6\bullet 2I_2$, the I_2 vibration has shifted to lower energies near 110 cm^{-1}, which is frequently seen in spectra of extended polyiodides.[2,4] This suggests that even at room temperature (where the I_2–I^- distance is slightly greater than 3.3 Å) this material is best thought of as a polyiodide. The material $(GUA)_8(PtI_6)_3[PtI_4(I_3)_2]\bullet 2I_2$, which has both I_2 molecules as well as I_3^- moieties, displays an expected Raman spectrum with vibrations at both 180 cm^{-1} and 125 cm^{-1}. For $(DMA)_3PtI_6(I_3)$, the expected I_3^- vibration near 125 cm^{-1} is present, in addition to a peak near 110 cm^{-1} that is seen in Raman spectra of longer chain oligoiodides,[2] and 140 cm^{-1}, which is seen in Raman spectra for symmetric I_3^- containing compounds.[31] In this respect, both $(GUA)_8(PtI_6)_3[PtI_4(I_3)_2]\bullet 2I_2$ and $(DMA)_3PtI_6(I_3)$ are best considered oligoiodide networks.

The optical absorption spectra of the three new poly/oligoiodide compounds, as well as their parent compounds, are presented in Figure 3 (b). We observe similar optical properties for all materials tested, as was previously observed for the A_2PtI_6 series.[16] For these platinum based compounds, the charge-transfer absorption of the $[PtI_6]^{2-}$ moieties dominates, regardless of structure. However, one clear difference is the increased absorption in the higher energy (2.5 eV – 3.75 eV) of the spectra of $(FA)_2PtI_6\bullet 2I_2$ and $(GUA)_8(PtI_6)_3[PtI_4(I_3)_2]\bullet 2I_2$. This increased absorption is caused by the higher-energy states of the I_2 molecules that lie above the platinum d e_g states. The band structure of $(FA)_2PtI_6\bullet 2I_2$ displays the typical underestimation of band gap when compared with experiment.†

Lastly, Figure 4 (a) displays the electron localization function (ELF) around iodine atoms and ions in $(FA)_2PtI_6\bullet 2I_2$, projected on the structure, on the plane that contains the infinite polyiodide chains. The lone pair lobes around the I_2 units are arranged axially along I^-–I_2–I^-, suggesting potential covalency in the interaction with the lone pairs on the I^- anions. Significant differences in the shape of the localization between the apical iodides of the $[PtI_6]^{2-}$ octahedra, and the four equatorial iodides not a part of

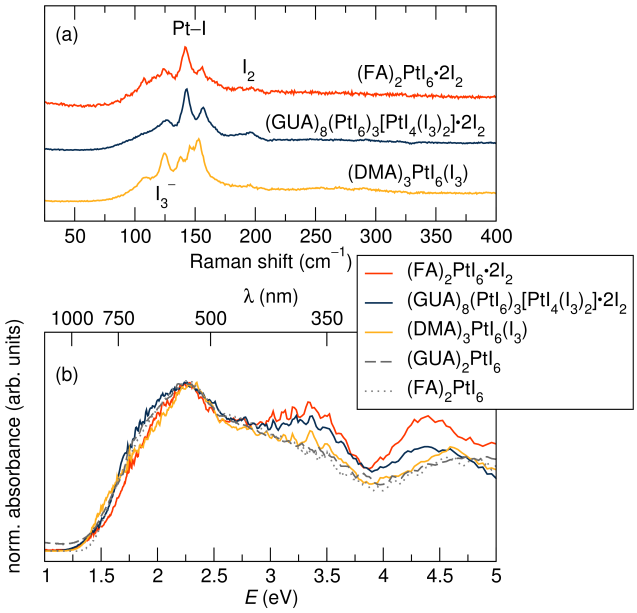

Fig. 3 (a) Raman spectra of the poly/oligoiodide materials. (b) Normalized optical absorption spectra (following Kubelka-Munk transformation of diffuse reflectance spectra) for the poly/oligoiodide materials. The spectra of the parent compounds $(FA)_2PtI_6$ and $(GUA)_2PtI_6$ are included for comparison.

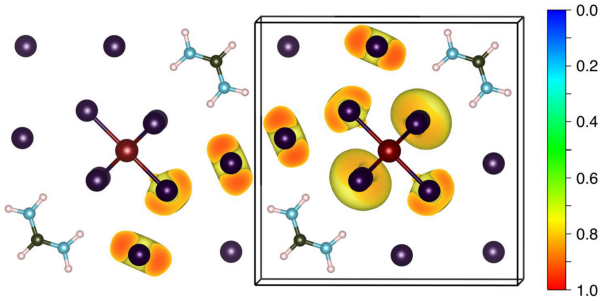

Fig. 4 Crystal structure of $(FA)_2PtI_6{\bullet}2I_2$ depicted in the plane containing the infinite polyiodide chains. The ELF is displayed for an isosurface value of 0.8, showing the lone pairs around select iodide ions and I_2 moieties.

the 1D polyiodide chain, are also seen, suggesting that the apical iodides are indeed involved in some degree of bond formation within this 1D chain. Furthermore, we present the electrostatic potential for $(FA)_2PtI_6{\bullet}2I_2$ in the ESI, showing subtle evidence of σ-holes on the I_2 molecules.† Given the appropriate angle and direction of the I–I···I and N–H···I bonds and the possible σ-hole, there is potential for halogen bonding stabilizing the observed structure of $(FA)_2PtI_6{\bullet}2I_2$.

In conclusion, we have presented three new hybrid platinum iodide compounds that emphasize the tendency of iodine and iodide to catenate, even when the iodide is part of a complex anion. Hydrogen bonding appears to play a large role in stabilizing the observed structures.

Conflicts of interest

There are no conflicts to declare.

Acknowledgments

This work was supported by the U.S. Department of Energy, Office of Science, Basic Energy Sciences under award number DE-SC-0012541. The use of the Shared Experimental Facilities of the Materials Research Science and Engineering Center (MRSEC) at UCSB is gratefully acknowledged (NSF DMR 1720256). We additionally acknowledge the Center for Scientific Computing at UCSB (NSF CNS-1725797 and NSF DMR-1720256). DHF thanks the National Science Foundation Graduate Research Fellowship Program for support (DGE 1144085). AKC thanks the Ras al Khaimah Centre for Advanced Materials for financial support. We thank an anonymous referee for advice on halogen bonding.

Notes and references

1 D. M. P. Mingos, *Essential Trends in Inorganic Chemistry*, Oxford University Press Oxford, 1998.
2 P. H. Svensson and L. Kloo, *Chem. Rev.*, 2003, **103**, 1649–1684.
3 S. A. Adonin, M. N. Sokolov and V. P. Fedin, *Coord. Chem. Rev.*, 2018, **367**, 1–17.
4 S. Madhu, H. A. Evans, V. V. T. DoanâĂŘNguyen, J. G. Labram, G. Wu, M. L. Chabinyc, R. Seshadri and F. Wudl, *Angew. Chemie Int. Ed.*, 2016.
5 A. J. Heeger, S. Kivelson, J. R. Schrieffer and W.-P. Su, *Rev. Mod. Phys.*, 1988, **60**, 781.
6 A. Hagfeldt and M. Grätzel, *Acc. Chem. Res.*, 2000, **33**, 269–277.
7 B. Li, L. Wang, B. Kang, P. Wang and Y. Qiu, *Sol. Energy Mater. Sol. Cells*, 2006, **90**, 549–573.
8 E. A. Gibson, *Chem. Soc. Rev.*, 2017, **46**, 6194–6209.
9 G. Zhang, M. Zhang, X. Ye, X. Qiu, S. Lin and X. Wang, *Adv. Mater.*, 2014, **26**, 805–809.
10 Y. Zhao and K. Zhu, *Chem. Soc. Rev.*, 2016, **45**, 655–689.
11 D. H. Fabini, J. G. Labram, A. J. Lehner, J. S. Bechtel, H. A. Evans, A. Van der Ven, F. Wudl, M. L. Chabinyc and R. Seshadri, *Inorg. Chem.*, 2016, **56**, 11–25.
12 B. Saparov and D. B. Mitzi, *Chem. Rev.*, 2016, **116**, 4558–4596.
13 W. Zhang, X. Liu, L. Li, Z. Sun, S. Han, Z. Wu and J. Luo, *Chem. Mater.*, 2018, **30**, 4081–4088.
14 A. J. Lehner, D. H. Fabini, H. A. Evans, C.-A. Hébert, S. R. Smock, J. Hu, H. Wang, J. W. Zwanziger, M. L. Chabinyc and R. Seshadri, *Chem. Mater.*, 2015, **27**, 7137–7148.
15 T. A. Shestimerova, N. A. Yelavik, A. V. Mironov, A. N. Kuznetsov, M. A. Bykov, A. V. Grigorieva, V. V. Utochnikova, L. S. Lepnev and A. V. Shevelkov, *Inorg. Chem.*, 2018, **57**, 4077–4087.
16 H. A. Evans, D. H. Fabini, J. L. Andrews, M. Koerner, M. B. Preefer, G. Wu, F. Wudl, A. K. Cheetham and R. Seshadri, *Inorg. Chem.*, 2018, **57**, 10375–10382.
17 A. N. Usoltsev, S. A. Adonin, P. A. Abramov, A. S. Novikov, V. R. Shayapov, P. E. Plyusnin, I. V. Korolkov, M. N. Sokolov and V. P. Fedin, *Eur. J. Inorg. Chem.*, 2018, **2018**, 3264–3269.
18 T. A. Shestimerova, N. A. Golubev, N. A. Yelavik, M. A. Bykov, A. V. Grigorieva, Z. Wei, E. V. Dikarev and A. V. Shevelkov, *Cryst. Growth Des.*, 2018, **18**, 2572–2578.
19 M. Berkei, J. F. Bickley, B. T. Heaton and A. Steiner, *Chem. Commun.*, 2002, 2180–2181.
20 D. Schneider, A. Schier and H. Schmidbaur, *Dalt. Trans.*, 2004, 1995–2005.
21 K. F. Purcell and J. C. Kotz, *An Introduction to Inorganic Chemistry*, Holt Rinehart & Winston, 1980.
22 R. E. Wasylishen, O. Knop and J. B. Macdonald, *Solid State Commun.*, 1985, **56**, 581–582.
23 A. Poglitsch and D. Weber, *J. Chem. Phys.*, 1987, **87**, 6373–6378.
24 M. T. Weller, O. J. Weber, J. M. Frost and A. Walsh, *J. Phys. Chem. Lett.*, 2015, **6**, 3209–3212.
25 D. H. Fabini, C. C. Stoumpos, G. Laurita, A. Kaltzoglou, A. G. Kontos, P. Falaras, M. G. Kanatzidis and R. Seshadri, *Angew. Chemie Int. Ed.*, 2016, **55**, 15392–15396.
26 G. Cavallo, P. Metrangolo, R. Milani, T. Pilati, A. Priimagi, G. Resnati and G. Terraneo, *Chem. Rev.*, 2016, **116**, 2478–2601.
27 K. N. Robertson, T. S. Cameron and O. Knop, *Can. J. Chem.*, 1996, **74**, 1572–1591.
28 T. Steiner, *Acta Crystallogr. Sect. B*, 1998, **54**, 456–463.
29 H. Hamaguchi, *J. Chem. Phys.*, 1978, **69**, 569–578.
30 P. Deplano, F. A. Devillanova, J. R. Ferraro, F. Isaia, V. Lippolis and M. L. Mercuri, *Appl. Spectrosc.*, 1992, **46**, 1625–1629.
31 P. H. Svensson and L. Kloo, *J. Chem. Soc. Dalt. Trans.*, 2000, 2449–2455.

Supporting Information:

The capricious nature of iodine catenation in I_2 excess, perovskite-derived hybrid Pt(IV) compounds

E-mail:

Hayden A. Evans,[ab] Jessica L. Andrews,[a] Douglas H. Fabini,[bc‡] Molleigh B. Preefer,[ab] Guang Wu,[a] Anthony K. Cheetham,[d] Fred Wudl,[c] and Ram Seshadri[abc]

[a]*Department of Chemistry and Biochemistry, University of California Santa Barbara, California 93106 United States. E-mail: seshadri@mrl.ucsb.edu* [b]*Materials Research Laboratory, University of California Santa Barbara, California 93106 United States* [c]*Materials Department, University of California Santa Barbara, California 93106 United States* [d]*Department of Materials Science and Engineering, National University of Singapore, Singapore 117575, Singapore* ‡*Present address: Department of Nanochemistry, Max Planck Institute for Solid State Research, Heisenbergstr. 1, 70569 Stuttgart, Germany*

Experimental Information

The hydroiodic acid (HI, 57% wt/wt in aqueous solution, Spectrum) used for the following reactions did not contain the reducing stabilizer hypophosphorous acid (H_3PO_2). The free iodine in solution (that forms when hydroiodic acid is exposed to air) is needed for the $(FA)_2PtI_6 \bullet 2I_2$ and $(GUA)_8(PtI_6)_3[PtI_4(I_3)_2] \bullet 2I_2$ preparations, and is also thought to be responsible for the oxidation of Pt^{2+} to Pt^{4+} during $(DMA)_3PtI_6(I_3)$ preparation.

$(FA)_2PtI_6 \bullet 2I_2$ was prepared by placing 50 mg of $(FA)_2PtI_6$ crystals in a sealed vial with a small amount of HI. The preparation of $(FA)_2PtI_6$ can be found in our previous publication.[1] If replicated, the amount of HI included should be just enough to cover all $(FA)_2PtI_6$ crystals. This mixture was left to recrystallize for at least one month, but can proceed longer if bronze $(FA)_2PtI_6$ crystals are still seen after that time. The originally bronze, metallic-looking $(FA)_2PtI_6$ crystals will become black crystals of $(FA)_2PtI_6 \bullet 2I_2$. We note that we were unable to prepare $(FA)_2PtI_6 \bullet 2I_2$ by exposing $(FA)_2PtI_6$ crystals to either iodine vapor or an iodine solution (H_2O or organic solvent). Once the crystals of $(FA)_2PtI_6 \bullet 2I_2$ are filtered, do not wash with solvents as these will destroy the crystals. It was found best to gently dry them on filter paper, and leave for a few days to dry out.

$(GUA)_8(PtI_6)_3[PtI_4(I_3)_2] \bullet 2I_2$ was prepared following the same procedure for the preparation of $(FA)_2PtI_6 \bullet 2I_2$. These crystals will also degrade with most solvents. The preparation of $(GUA)_2PtI_6$ can be found in our previous publication.[1]

$(DMA)_3PtI_6(I_3)$ was prepared by combining 99.30 mg DMAI (0.561 mmol, Sigma Aldrich, 98%) and 50 mg (0.187 mmol) $PtCl_2$ (Strem, 99.9%) in 8.0 g unstablized HI, and heated to dissolve any solid that initially formed. This solution was heated for 15 min. The solution then was slowly cooled to room temperature, where black plate habit crystals of $(DMA)_3PtI_6(I_3)$ form. These crystals were vacuum filtered, washed with diethyl ether, and vacuum-dried overnight.

Single crystal X-ray diffraction data was collected on a Bruker KAPPA APEX II diffractometer equipped with an APEX II CCD detector using a TRIUMPH monochromator with

a Mo Kα X-ray source (λ = 0.71073 Å). The crystals were mounted on a cryoloop under Paratone-N oil and kept under nitrogen. Absorption correction of the data was carried out using the multiscan method as implemented in SADABS.[2] Subsequent calculations were carried out using SHELXTL.[3] Structure determination was done using intrinsic methods. All hydrogen atom positions were omitted. Structure solution, refinement, and creation of publication data was performed using SHELXTL. Crystal structures were visualized using the VESTA software suite.[4]

Powder X-ray diffraction was performed on a Panalytical Empyrean Powder Diffractometer (Bragg-Brentano HD module, no monochromator) equipped with a Cu source λ = 1.5418 Å. Rietveld refinements were performed in the TOPAS software suite.[5]

A Shimadzu UV3600 UV-NIR Spectrometer was used to gather data in diffuse reflectance mode. The title compounds tested were suspended in $BaSO_4$ medium (*via* grinding). The reflectance spectra were Kubelka-Munk transformed for relative absorbance spectra.

Thermogravimetric analysis (TGA) on all compounds was conducted using a TA Instruments Discovery instrument. A rate of 25 cm^3/min dry nitrogen purge was employed with a temperature ramp rate of 10°C/min. The maximum temperature of the experiment was 900°C.

Differential scanning calorimetry (DSC) measurements were performed using a TA Q2000 calorimeter. Samples (2 mg to 10 mg each) were hermetically sealed inside TZero aluminum pans. Samples were first cooled to −150°C, then heated at 10 °C/min. This was repeated for three cycles.

Electronic structure calculations for $(FA)_2PtI_6 \bullet 2I_2$ were performed with the Vienna Ab initio Simulation Package (VASP),[6–9] which implements the KohnSham formulation of density functional theory (DFT) using a plane wave basis set and the projector augmented wave formalism.[10,11] The generalized gradient approximation was employed using the exchange and correlation functional of Perdew, Burke, and Ernzerhof (GGAPBE).[12] The plane

wave basis set cutoff energy (800 eV) and k-point mesh density (∼1500 k-points per reciprocal atom for convergence of the charge density, ∼40,000 k-points per reciprocal atom for computing the density of states, all Γ-centered Monkhorst-Pack sampling)[13] were chosen based on convergence of the total energy. Structure relaxation was performed, including van der Waals corrections (DFT-D3 method of Grimme,[14] to a force tolerance of 4 meV Å^1. The relaxed structure preserved the space group symmetry observed in experiment. The Brillouin zone path was that of Setyawan and Curtarolo.[15] The electrostatic potential was visualized on isosurfaces of the valence charge density with custom python code using the improved marching cubes algorithm of Lewiner and coworkers as implemented in the skimage package.[16]

Material descriptions

All structures reported were solved via single crystal X-ray diffraction with relevant crystallographic data summarized in Tables S1 and S2, and structures with 95% elipsoids in Figures S1 - S4. The CCDC deposition numbers are 1864903 – 1864907.

The B alerts in the low and room temperature data sets for $(FA)_2PtI_6{\bullet}2I_2$ data originate from the close I_2 – I^- anion distances. We discuss this in the main text as the formation of a 1D polyiodide chain.

The B alerts in the 100 K data set for $(GUA)_8(PtI_6)_3[PtI_4(I_3)_2]{\bullet}2I_2$ pertain to the close I_2 to I^- anions distances which we describe as secondary bonding associations in the main text.

The B alerts in both $(DMA)_3PtI_6(I_3)$ data sets come from the omitted hydrogen atoms which were not included due to the disorder of the organic cation atom sites. Hydrogens were included on the N site of the ordered DMA cation. There is one B alert in the 100 K data set which is due to secondary bond associations between I_3^- to I^- anions.

Table S1: Crystallographic Data for $(FA)_2PtI_6 \bullet 2I_2$ and $(GUA)_8(PtI_6)_3[PtI_4(I_3)_2] \bullet 2I_2$

Empirical Formula	$[CH(NH_2)_2]PtI_6 \bullet 2I_2$		$[C(NH_2)_3]_8(PtI_6)_3[PtI_4(I_3)_2] \bullet 2I_2$
Crystal habit, color	block, black		block, black
Crystal system	tetragonal	tetragonal	triclinic
Space group (#)	$P4_2/mnm$ (136)	$P4_2/mnm$ (136)	$P\bar{1}$ (2)
Volume (Å^3)	1178.6(4)	1200.3(16)	2176(3)
T (K)	100	270	108
a (Å)	12.340(2)	12.379(7)	12.768(9)
b (Å)	12.340(2)	12.379(7)	13.016(9)
c (Å)	7.728(1)	7.833(5)	14.52(1)
α (°)	90	90	110.55(2)
β (°)	90	90	102.74(2)
γ (°)	90	90	93.87(2)
Z	2	2	1
ρ (g mol^{-1})	1554.23	1554.23	5321.86
Dens. (g cm^{-3})	4.379	4.328	4.061
Abs. (mm^{-1})	19.040	18.698	17.793
F_{000}	1316	1336	2272
Reflections (unique)	6507 (1005)	3456 (995)	9573 (4834)
R_{int}	0.0258	0.0574	0.1981
R_1	0.0217	0.0337	0.0817
wR_R	0.0412	0.0408	0.1936
∂F (eÅ^{-3})	1.117 & −6.062	1.132 & −1.266	4.382 & −4.836
GOF	1.102	1.208	0.939

Table S2: Crystallographic Data for $(DMA)_3PtI_6(I_3)$.

Empirical Formula	$[NH_2(CH_3)_2]_3PtI_6(I_3)$	
Crystal habit, color	block, black	
Crystal system	monoclinic	monoclinic
Space group (#)	$C2/m$ (12)	$C2/m$ (12)
Volume (Å^3)	1342.5(1)	1414.3(3)
T (K)	100	264
a (Å)	16.768(9)	17.012(2)
b (Å)	7.666(4)	7.8309(9)
c (Å)	10.656(6)	10.837(2)
α (°)	90	90
β (°)	101.46(2)	101.705(8)
γ (°)	90	90
Z	2	2
ρ (g mol^{-1})	1475.47	1475.47
Dens. (g cm^{-3})	3.650	3.465
Abs. (mm^{-1})	15.570	14.779
F_{000}	1272	1272
Reflections (unique)	3470 (2107)	4293 (2297)
R_{int}	0.0980	0.1329
R_1	0.0634	0.0580
wR_R	0.1348	0.0791
∂F (eÅ^{-3})	3.384 & -5.871	3.407 & -1.727
GOF	1.062	1.533

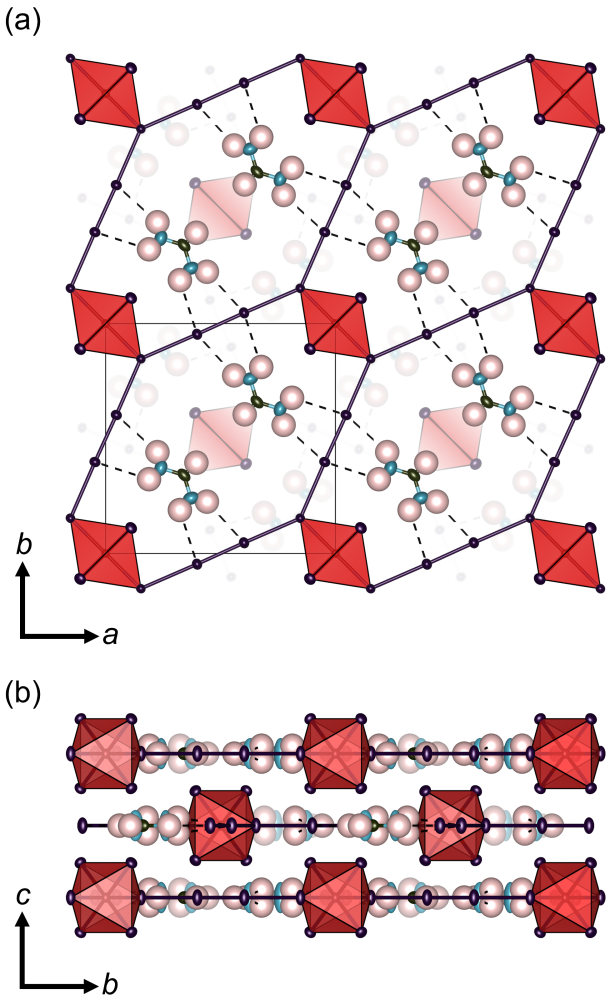

Figure S1: Crystal structure of $(FA)_2PtI_6 \bullet 2I_2$ at 100 K with displacement ellipsoids (95% probability). (a) Depiction of the 1D chains forming between the iodide on the $[PtI_6]^{2-}$ octahedra and I_2 molecules. Hydrogen bonding columns that form between the FA cations and the I_2 molecules are displayed with dashed lines. The pertinent bond lengths are: I_2 molecule 2.77 Å; I_2–I^- 3.29 Å; N-H$\cdots$$I_2$ 3.0 Å. (b) Side view of the 2D sheets that are found parallel to the ab plane.

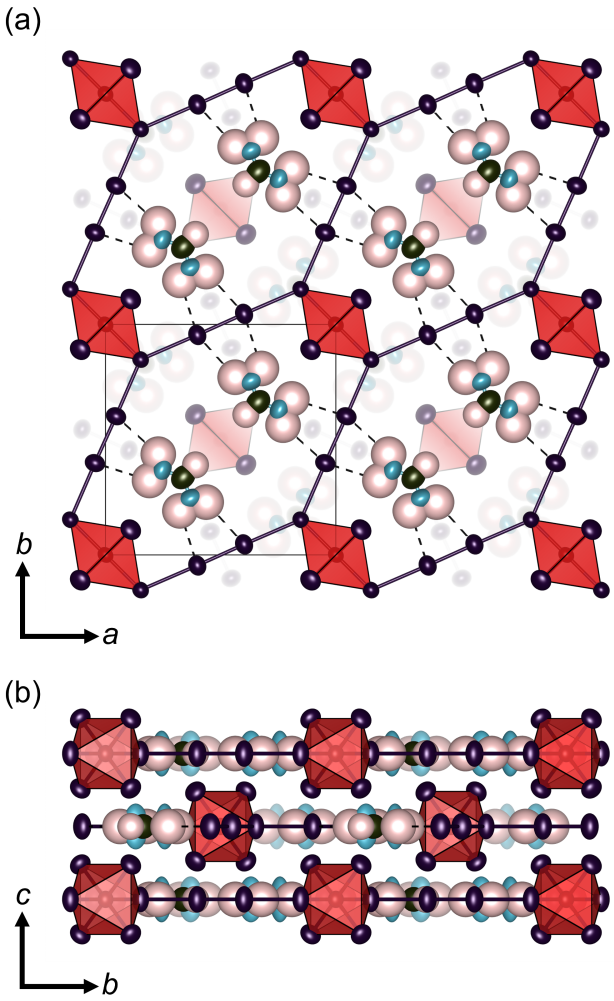

Figure S2: Crystal structure of $(FA)_2PtI_6 \bullet 2I_2$ at 260 K with displacement ellipsoids (95% probability). (a) Depiction of the 1D chains forming between the iodide on the $[PtI_6]^{2-}$ octahedra and I_2 molecules. Hydrogen bonding columns that form between the FA cations and the I_2 molecules are displayed with dashed lines. The pertinent bond lengths are: I_2 molecule 2.76 Å; I_2–I^- 3.32 Å; N-H$\cdots$$I_2$ 3.05 Å. (b) Side view of the 2D sheets that are found parallel to the ab plane.

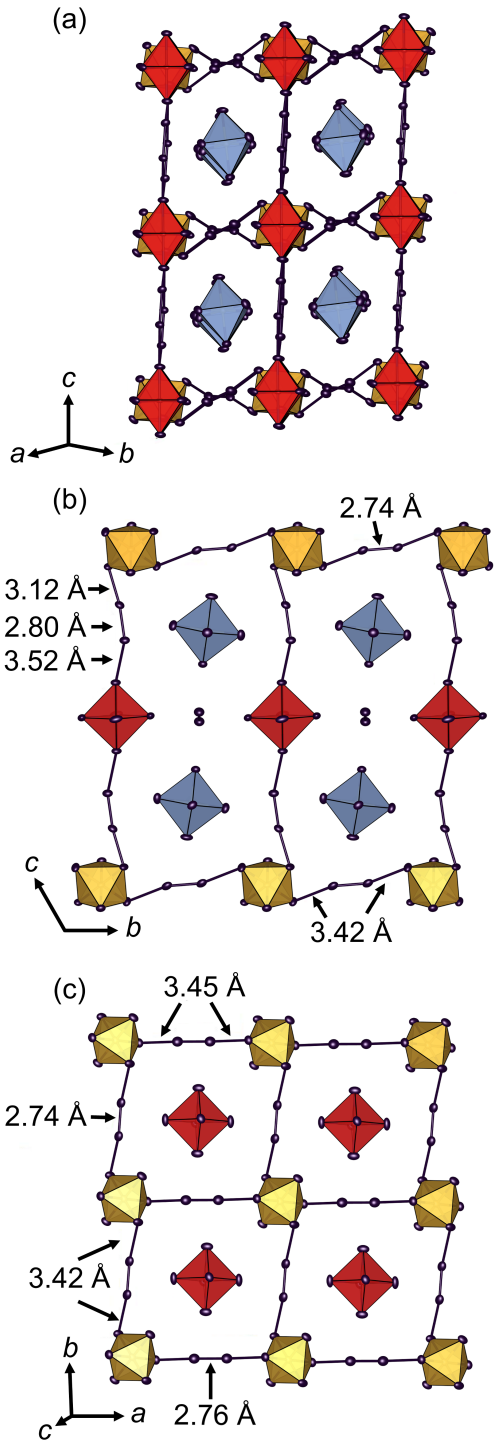

Figure S3: Crystal structure of $(GUA)_8(PtI_6)_3[PtI_4(I_3)_2]\bullet 2I_2$ at 100 K with displacement ellipsoids (95% probability). (a) Depiction of the $(GUA)_8(PtI_6)_3[PtI_4(I_3)_2]\bullet 2I_2$ structure with organic cations omitted. (b) Top down view of the cb-plane of $(GUA)_2PtI_6\bullet I_2$, demonstrating the secondary iodide bonding network that forms between **2** and **3**. The I_3 moieties of **3** run perpendicular to the b-axis, and link with **2**. The I_2 molecules seen in between **1** and **2** in this view are the I_2 molecules that link **3** along the a-axis seen in (c). (c) Top down view of the secondary bonding axis in the ab-plane, which forms between I_2 molecules and the four equatorial I^- iodides of **3**.

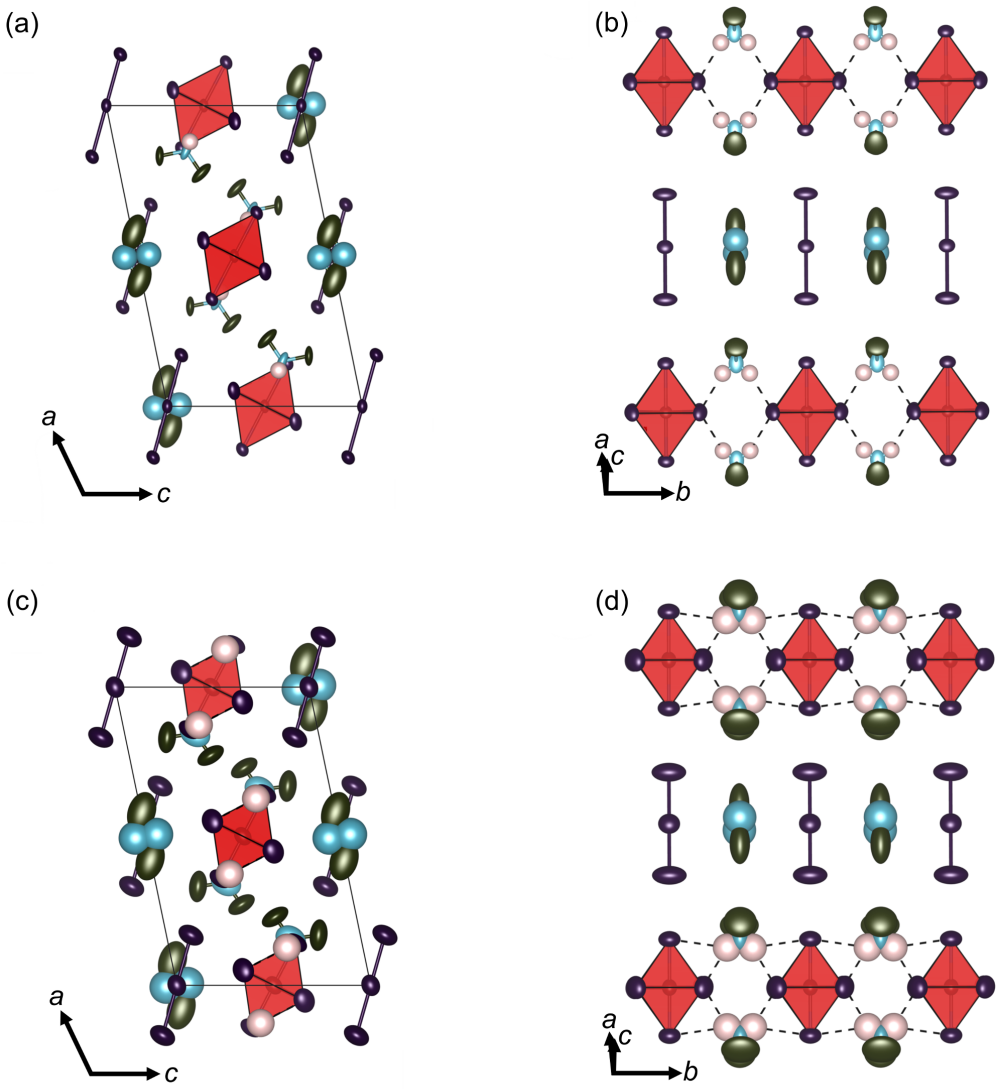

Figure S4: Crystal structure of $(DMA)_3PtI_6(I_3)$ at 100 K [(a) and (b)] and 264 K [(c) and (d)] with displacement ellipsoids (95% probability). (a) View of $(DMA)_3PtI_6(I_3)$ down the b-axis. (b) View of $(DMA)_3PtI_6(I_3)$ depicting the hydrogen bonding interactions between DMA cations and $[PtI_6]^{2-}$ octahedra, as well as the arrangement of I_3^- anions relative to the nearby $[PtI_6]^{2-}$ octahedra. The distance between apical $[PtI_6]^{2-}$ iodides and nearby I_3^- is 3.49 Å. (c) View of $(DMA)_3PtI_6(I_3)$ down the b-axis. (d) View of $(DMA)_3PtI_6(I_3)$ depicting the hydrogen bonding interactions between DMA cations and $[PtI_6]^{2-}$ octahedra, as well as the arrangement of I_3^- anions relative to the nearby $[PtI_6]^{2-}$ octahedra. The distance between apical $[PtI_6]^{2-}$ iodides and nearby I_3^- is 3.56 Å.

Proposed hydrogen bonding network of $(GUA)_8(PtI_6)_3[PtI_4(I_3)_2]\bullet 2I_2$

The following figures illustrate the proposed hydrogen bonding network that exists in $(GUA)_8(PtI_6)_3[PtI_4(I_3)_2]\bullet 2I_2$. Due to the overall small contribution to the SXRD dataset that the N and C atoms provide, it is difficult to say that the reported GUA cation positions are definitive. *However*, the hydrogen bonding network that forms using the isotropic positions of the N atoms and their respective H atoms, looks uncannily similar to the network seen in the parent compound of $(GUA)_8(PtI_6)_3[PtI_4(I_3)_2]\bullet 2I_2$, $(GUA)_2PtI_6$. Namely, each of the six hydrogens of the GUA cations point towards nearby I^- on $[PtI_6]^{2-}$ octahedra. In order to deconstruct this complex network of hydrogen bonding, Figures S5–S7 describe the suspected hydrogen bonding network formed by the four crystallographically distinct GUA cations. The cations are labeled GUA1 through GUA4, and coincide with the .cif atom labels as such GUA1 = C1, N1, H1a, H1b, N2, H2a, H2b, N3, H3a, H3b, etc in sequential order. GUA2 and GUA4 are included together to emphasize that their bonding preferences are the same, i.e. the hydrogen bonding network forms only with the Pt octahedra **1** and **2**. Interestingly, unlike the hydrogen bonding network that forms in $(FA)_2PtI_6\bullet 2I_2$, the proposed network exists exclusively with $[PtI_6]^{2-}$, except for the GUA3 cation (Figure S7) which bonds with one of the I_3 molecules. The network has been drawn with a H$\cdots$I maximum of 3.3 Å, so as to account for other favorable, yet weaker, hydrogen bonding positions of the GUA cations.

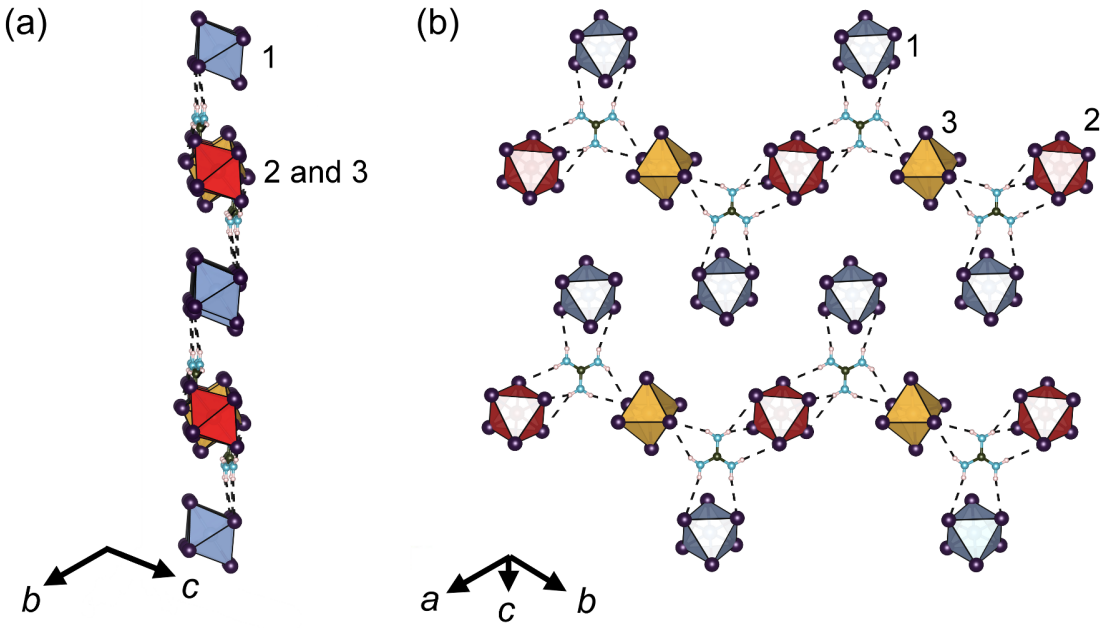

Figure S5: View of the hydrogen bonding network that forms between GUA1 and **1**, **2**, and **3**. The hydrogen bonding that occurs between GUA1 and **3** occurs between two of the four equitorial I^-, not any of the I atoms of the I_3 moiety, which is excluded for clarity.

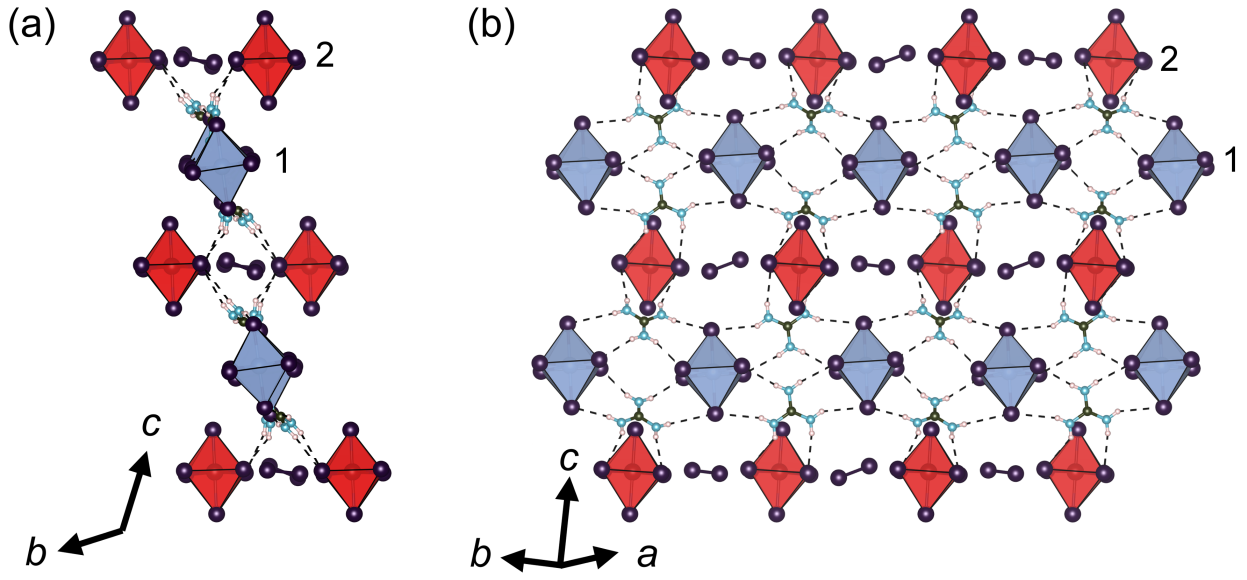

Figure S6: View of the hydrogen bonding network that forms between GUA2/GUA4 and the Pt species, **1** and **2**. This network illustrates that even though **1** and **2** are not linked via a secondary iodide bonding network, that they are extensively coupled via the hydrogen bonding network.

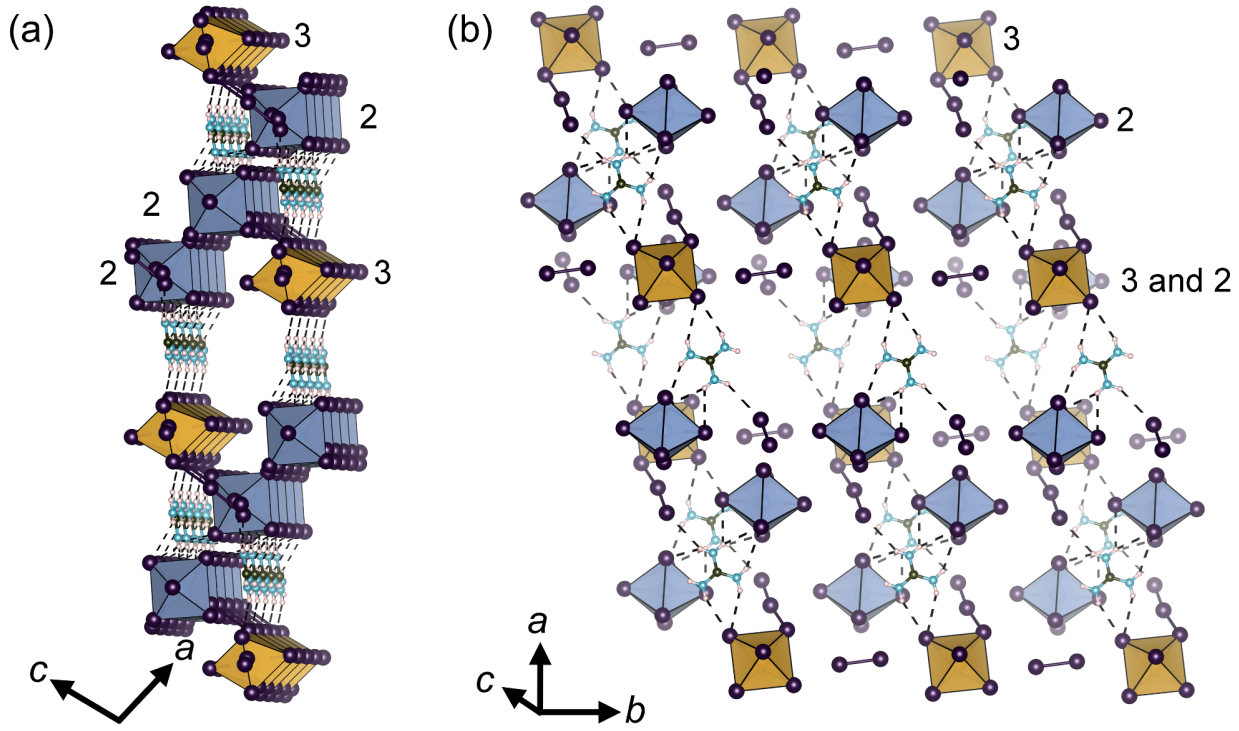

Figure S7: View of the hydrogen bonding network that forms between GUA3, and the Pt species, **1** and **3**. GUA3 forms one hydrogen bond with the terminal I atom of the I_3 moiety.

Powder X-ray Diffraction

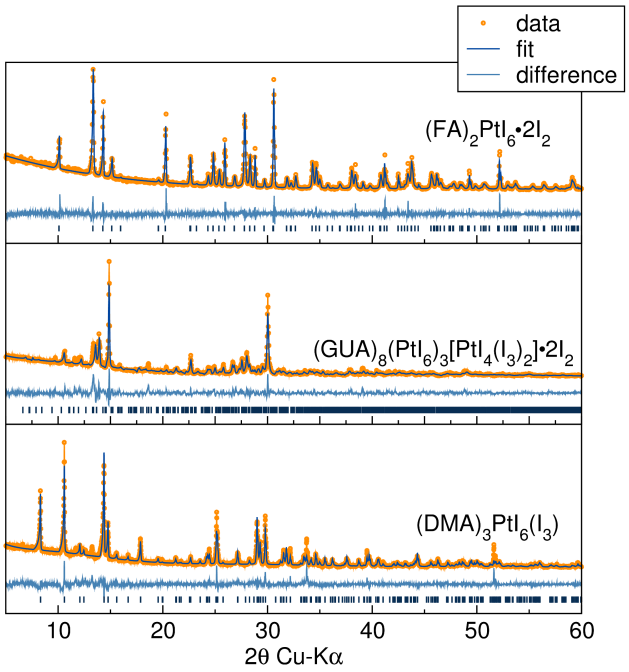

Figure S8: Rietveld refinements of the title compounds.

Table S3: Refined lattice parameters of title compounds.

Forumla	$(FA)_2PtI_6 \bullet 2I_2$	$(GUA)_8(PtI_6)_3[PtI_4(I_3)_2] \bullet 2I_2$	$(DMA)_3PtI_6(I_3)$
a (Å)	12.402	12.683	17.030
b (Å)	12.402	13.045	7.840
c (Å)	7.865	14.628	10.841
α (°)	90	109.54	90
β (°)	90	102.81	101.75
γ (°)	90	94.11	90

Experimental laboratory PXRD data was Rietveld refined (without atomic occupancy) using room temperature single crystal diffraction as the structural comparison (Figure S8). The refinements indicate that the each bulk sample has unit cell parameters close to single crystal diffraction dimensions (Table S3 refined data, Tables S1 and S2 for single crystal data).

Thermogravimetric Analysis (TGA)

Thermogravimetric analysis of the title compounds are presented in Figures S9 - S11. The degradation profiles of $(FA)_2PtI_6 \bullet 2I_2$ and $(GUA)_8(PtI_6)_3[PtI_4(I_3)_2] \bullet 2I_2$ are quite similar, in that they show a multistep evolution including the release of I_2 near 100 °C until 300 °C. The degradation profile of $(DMA)_3PtI_6(I_3)$ occurs in one step near 210 °C.

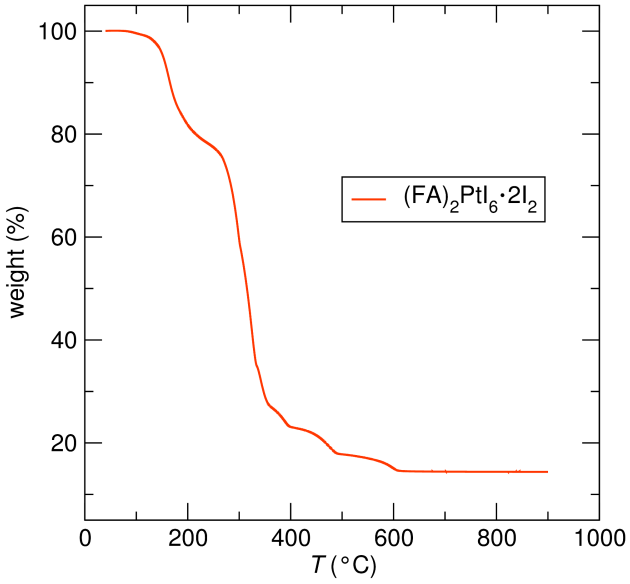

Figure S9: TGA data for $(FA)_2PtI_6 \bullet 2I_2$ from room temperature to 900°C.

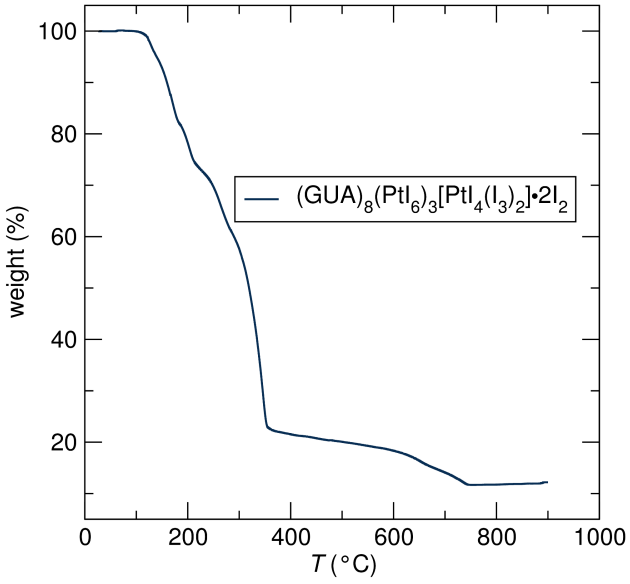

Figure S10: TGA data for $(GUA)_8(PtI_6)_3[PtI_4(I_3)_2] \bullet 2I_2$ from room temperature to 900°C.

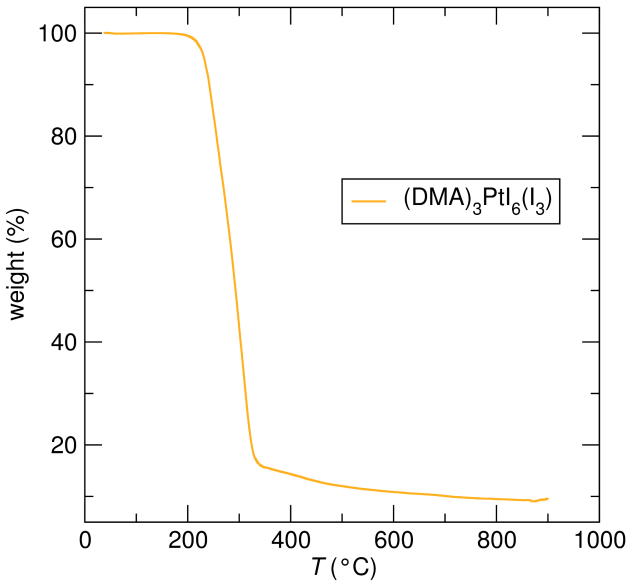

Figure S11: TGA data for $(DMA)_3PtI_6(I_3)$ from room temperature to 900°C.

Differential Scanning Calorimetry (DSC)

Differential scanning calorimetry of the title compounds are presented in Figures S12 - S14. All materials display no observable first order phase transition.

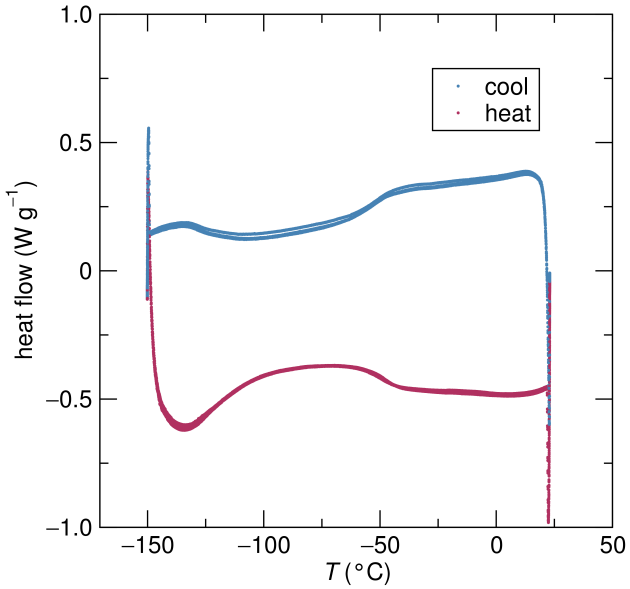

Figure S12: DSC data for $(FA)_2PtI_6{\bullet}2I_2$ between −150 °C and 25 °C.

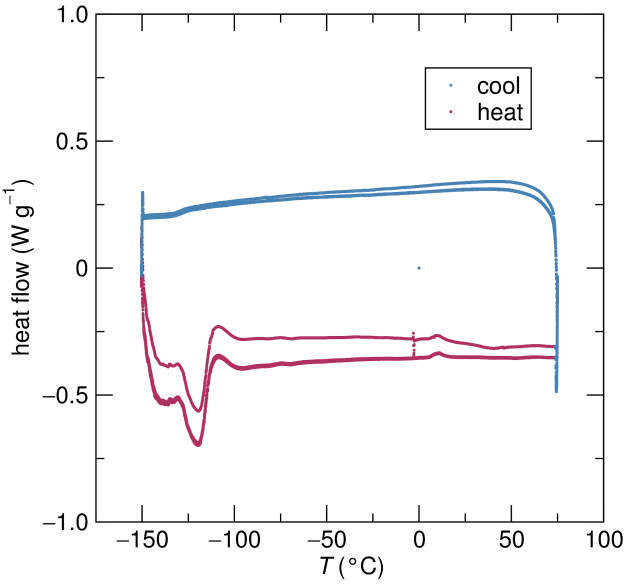

Figure S13: DSC data for $(GUA)_8(PtI_6)_3[PtI_4(I_3)_2]\bullet 2I_2$ between −150 °C and 75 °C.

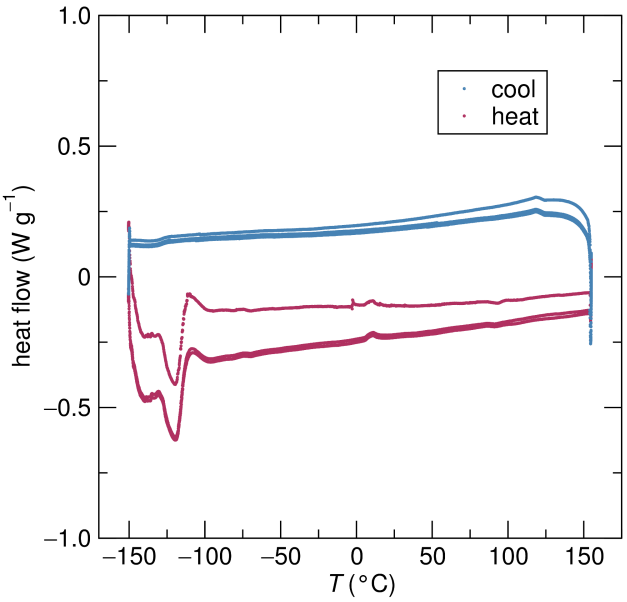

Figure S14: DSC data for $(DMA)_3PtI_6(I_3)$ between −150 °C and 150 °C.

Band Structure and Density of States

Band structure and density of states for the compound $(FA)_2PtI_6\bullet 2I_2$ are illustrated in Figure S15. Clearly noted is the disperse conduction band, which is due to iodine/iodide

proximity, as well as the position of the empty I_2 states which lie above the Pt d e_g levels.

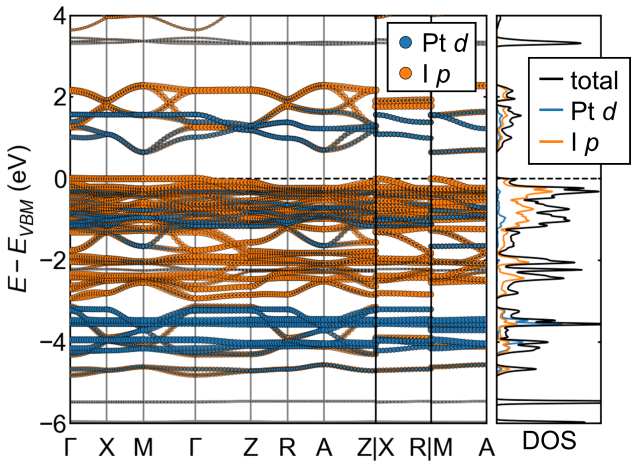

Figure S15: Band structure and density of states for the compound $(FA)_2PtI_6 \bullet 2I_2$.

Electrostatic potential examination

Visualized in Figure S16(a) is the crysal structure of $(FA)_2PtI_6 \bullet 2I_2$, (b) the electron localization function, and (c) the electrostatic potential visualized on isosurfaces of the valence charge density for $(FA)_2PtI_6 \bullet 2I_2$. We believe that Figure S16(c) is a an insightful way to view the electrostatic potential, as it shows how electro-/nucleo-philic the "surface" of each molecule is, rather than a slice through the interior of atoms. It is noted that the hydrogens on the FA cation are quite electrophilic (especially the N–H), hence their tendency to be hydrogen bond donors. Most interestingly, there is an electrophilic region along the I_2-axis which points towards the iodide of the $[PtI_6]^{2-}$ octahedra which is a part of the extended I chain. We believe this observation, in addition to the overall structural signatures (bond angles and distances) of each component moiety, is partial evidence for the existence of the σ-holes on the I_2 molecules, consistent with halogen bonding.[17–19]

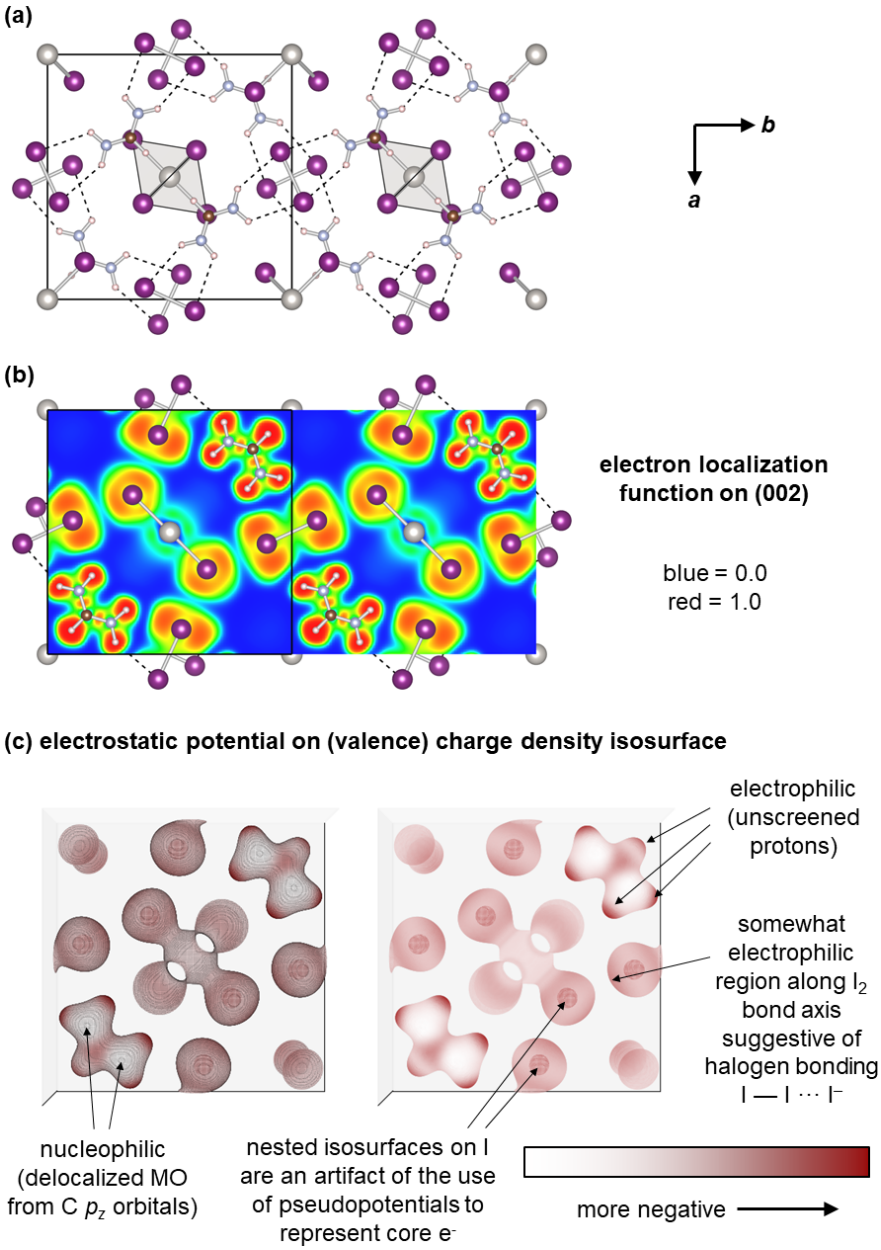

Figure S16: (a) The crystal structure of $(FA)_2PtI_6 \bullet 2I_2$, (b) the electron localization function, and (c) the electrostatic potential visualized on isosurfaces of the valence charge density for $(FA)_2PtI_6 \bullet 2I_2$. The color legend indicates the degree of negative electrostatic potential.

References

(1) H. A. Evans, D. H. Fabini, J. L. Andrews, M. Koerner, M. B. Preefer, G. Wu, F. Wudl, A. K. Cheetham, and R. Seshadri *Inorg. Chem.* 2018, **57**, 10375–10382.

(2) SADABS; G. M. Sheldrich, University of Gottingen: Germany, 2005.

(3) SHELXTL PC, Version 6.12; Bruker AXS Inc.: Madison, WI, 2005.

(4) K. Momma and F. Izumi. *Commission on Crystallogr. Comput.* 2006, **7**, 106–119.

(5) A. Coelho. *J. Appl. Cryst.* 2018, **51**, 210–218.

(6) G. Kresse and J. Hafner, *Phys. Rev. B*, 1993, **47**, 558–561.

(7) G. Kresse and J. Hafner, *Phys. Rev. B*, 1994, **49**, 14251–14269.

(8) G. Kresse and J. Furthmüller, *Phys. Rev. B*, 1996, **54**, 11169–11186.

(9) G. Kresse and J. Furthmüller, *Comput. Mater. Sci.*, 1996, **6**, 15–50.

(10) P. E. Blöchl, *Phys. Rev. B*, 1994, **50**, 17953–17979.

(11) G. Kresse, and D. Joubert, *Phys. Rev. B*, 1999, **59**, 1758–1775.

(12) J. P. Perdew, K. Burke and M. Ernzerhof, *Phys. Rev. Lett.*, 1997, **77**, 3865–3868.

(13) H. J. Monkhorst and J. D. Pack, *Phys. Rev. B*, **1976**, *13*, 5188–5192.

(14) S. Grimme, J. Antony, S. Ehrlich and H. Krieg, *J. Chem. Phys.*, 2010, **132**, 154104-1–154104-19.

(15) W. Setyawan and S. Curtarolo, *Comput. Mater. Sci.* 2010, **49**, 299–312.

(16) T. Lewiner, H. Lopes, A. Wilson Vieira and G. Tavares, *J. Graph. Tools*, 2003, **8**, 1–15.

(17) T. Clark, M. Hennemann, J. S. Murray, and P. Politzer, *J. Mol. Model.*, 2007, **13**, 291–296.

(18) P. Politzer, J. S. Murray, and T. Clark, *Phys. Chem. Chem. Phys.*, 2010, **12**, 7748–7757.

(19) Peter Politzer, J. S. Murray, T. Clark, and G. Resnati, *Phys. Chem. Chem. Phys.*, 2017, **19**, 32166–32178.